

Ballistic hot-electron transport in a quantum Hall edge channel defined by a double gate

Shunya Akiyama,¹ Taichi Hirasawa,¹ Yuya Sato,¹ Takafumi Akiho,² Koji Muraki,² and Toshimasa Fujisawa^{1,*}

¹*Department of Physics, Tokyo Institute of Technology, 2-12-1 Ookayama, Meguro, Tokyo, 152-8551, Japan.*

²*NTT Basic Research Laboratories, NTT Corporation, 3-1 Morinosato-Wakamiya, Atsugi 243-0198, Japan.*

(Dated: February 1, 2022)

Ballistic transport of hot electrons in a quantum Hall edge channel is attractive for studying electronic analog of quantum optics, where the edge potential profile is an important parameter that governs the charge velocity and scattering by longitudinal-optical (LO) phonons. Here we use a parallel double gate to control the electric field of the edge potential, and investigate the ballistic length of the channel by using hot-electron spectroscopy. The ballistic length is significantly enhanced by reducing the LO phonon scattering rate in the tailored potential.

Scattering of conduction electrons is crucial for studying novel quantum transport [1]. Scattering by impurities can be suppressed in high-mobility heterostructures, where cold electrons show ballistic electron transport with mean free path beyond $100 \mu\text{m}$ [2, 3]. The impurity scattering can also be evaded in quantum Hall edge channels under a strong magnetic field, where cold electrons travel along an equipotential line at the chemical potential even in the presence of impurities [4, 5]. Successful realizations of fermionic interferometers [6, 7] and quantum tomography [8] are promising for quantum information channels. While single-particle excitations relax into many-body excitations in a short distance as a result of electron-electron scattering with nearby channels [9–11], long coherence length of sub-millimeters was recently reported by tailoring the copropagating channel [12, 13]. On the other hand, the electron-electron scattering can also be suppressed significantly by exciting the electron of interest far above the chemical potential, where the hot electron in a soft edge potential of an AlGaAs/GaAs heterostructure cannot satisfy the momentum conservation for the scattering [14]. Long ballistic transport over millimeters is quite attractive particularly for studying electronic analog of quantum optics [15, 16]. For example, pure single-electron excitation with well-defined energy can be generated from a dynamic quantum dot [17]. The hot electron travels at velocity determined by the edge potential [18]. The energy and time uncertainties of a hot-electron wave packet can reach a level comparable to the quantum limit [19]. Channels for hot electrons can be tailored to implement a beam-splitter and a charge detector [20, 21]. In these experiments, the dominant scattering mechanism can be scattering by longitudinal optical (LO) phonons. Particularly for long ballistic transport, the phonon scattering should be suppressed by making the edge potential less steep, i.e., by lowering the edge electric field [14, 15, 22]. As the electric field also influences the hot-electron velocity, it would be better to

have tuning capability of the electric field. In most of the previous studies, an etching step covered with a flat gate was used to define edge channels [15, 18], so that little attention has been focused on the active tuning of the electric field.

Here we investigate ballistic hot-electron transport and LO phonon scattering in a tunable edge potential defined by two parallel fine gates along the channel. The scattering length is investigated by employing hot-electron spectroscopy with injector and detector point contacts. The scattering rate shows a non-monotonic energy dependence in agreement with electrostatic simulation. The double gate geometry can be used to tailor the edge potential for tuning the scattering as well as the velocity.

As shown in Fig. 1(a), a double gate with G_1 and G_2 was patterned on an AlGaAs/GaAs heterostructure. Large negative voltage V_{G1} on G_1 primary defines the right-moving edge channel under perpendicular magnetic field B , and small negative voltage V_{G2} on G_2 modifies the edge potential. To see its effect, we performed electrostatic calculations based on the Poisson equation by employing a two-dimensional (2D) finite element method with realistic parameters for our device [14, 23, 24]. For simplicity, we used the frozen surface model with a fixed charge density on the free surface [25]. The bulk region of the 2D electrons is regarded as a grounded metal, as the energy of hot electrons in this work (30 - 100 meV) is much higher than the Fermi energy of the 2D electrons ($\lesssim 10$ meV). The boundary position of the metallic region representing the 2D electron system was determined self-consistently in such a way that the charge density on the metallic region becomes zero at the boundary position.

With large negative V_{G1} applied while keeping $V_{G2} = 0$, the potential energy $e\phi(x)$ along the transverse axis x to the channel [see Fig. 1(a)] has a maximum underneath G_1 as shown by the black dashed line in Fig. 1(b). In a high magnetic field, this spatial profile can be regarded as that of the lowest Landau level (LLL). Hot electrons travel on the left side of the maximum at single-particle velocity $v_{\text{hot}} = E/B$, where $E = -d\phi/dx$ is the electric field. We focus on the LO phonon scattering within the

* fujisawa@phys.titech.ac.jp

LLL, where an electron emits the LO phonon energy of $\varepsilon_{\text{LO}} = 36$ meV with a spatial shift d between the initial and final states [22]. By neglecting the non-linearity in the potential for simplicity, the LO phonon scattering rate can be written as $\Gamma_{\text{LO}} = \Gamma_0 \exp(-d^2/2\ell_b^2)$, which depends strongly on $d \simeq \varepsilon_{\text{LO}}/eE$. Here, $\ell_b = \sqrt{\hbar/eB}$ is the magnetic length and Γ_0 is the form factor for the LO-phonon scattering. The scattering length $\ell_{\text{LO}} = v_{\text{hot}}/\Gamma_{\text{LO}}$ can be enhanced significantly by decreasing Γ_{LO} under the condition of $d \gtrsim \ell_b$, and thus by decreasing E . This can be done by applying negative V_{G2} ; as shown in Fig. 1(b), the slope of the potential energy $e\phi$, E , is reduced in a particular energy range that depends on V_{G2} . Figure 1(c) shows the potential energy $e\phi$ dependence of the calculated electric field E , where a clear dip in E develops as negative V_{G2} is applied. The impact on ℓ_{LO} at a representative magnetic field of $B = 9$ T is shown by the subsidiary scale (arbitrary unit). While this crude simulation can be used as a qualitative guide, huge enhancement of ℓ_{LO} is suggested with a small reduction of E . We investigate such potential tuning by measuring ℓ_{LO} in this work. We mainly focus on the LO phonon scattering within the LLL, while other mechanisms like electron-electron scattering and inter-Landau-level tunneling are important in some other conditions [14, 15, 26].

The LO phonon scattering length ℓ_{LO} is experimentally evaluated by using hot electron spectroscopy. As shown in the device geometry of Fig. 1(a) and the energy diagram of Fig. 2(a), hot electrons are injected from emitter E, which is biased at $eV_{\text{E}} = 10 - 200$ meV, through the injector point contact defined with gate G_{inj} . After traveling along the edge of the base (B) region, the electrons are analyzed with the detector point contact defined with gate G_{det} . Hot electrons with energy greater than the barrier height ε_{det} are introduced to the collector, while other electrons are reflected and lead to the base ohmic contact. The energy distribution function is obtained by measuring the collector current I_{col} or the reflected current I_{ref} as a function of gate voltage V_{det} on G_{det} which determines ε_{det} .

Since both G_1 and G_2 constitute the point contact in conjunction with G_{det} in our device as shown in Fig. 1(a), the potential modulation with G_2 also influences the detector characteristics. Figure 1(d) shows the approximate potential profile $\phi(x')$ along the transverse axis x' around the detector point contact [see Fig. 1(a)], where the wedge-shaped G_{det} is crudely approximated by an infinitely wide gate so as to fit with the 2D simulation. The potential minimum marked by the open circles corresponds to the barrier height or the saddle-point energy ε_{det} in the actual device. The simulation shows that ε_{det} increases with decreasing V_{det} . Figure 1(e) shows the relation between ε_{det} and V_{det} , where one can see that the slope, or the lever-arm factor $\alpha = \Delta\varepsilon_{\text{det}}/\Delta V_{\text{det}}$, changes abruptly at a particular point that depends on V_{G2} . The ε_{det} value at this bending point in Fig. 1(e) is close to the $e\phi$ value at the dip in Fig. 1(c). We also use this detector

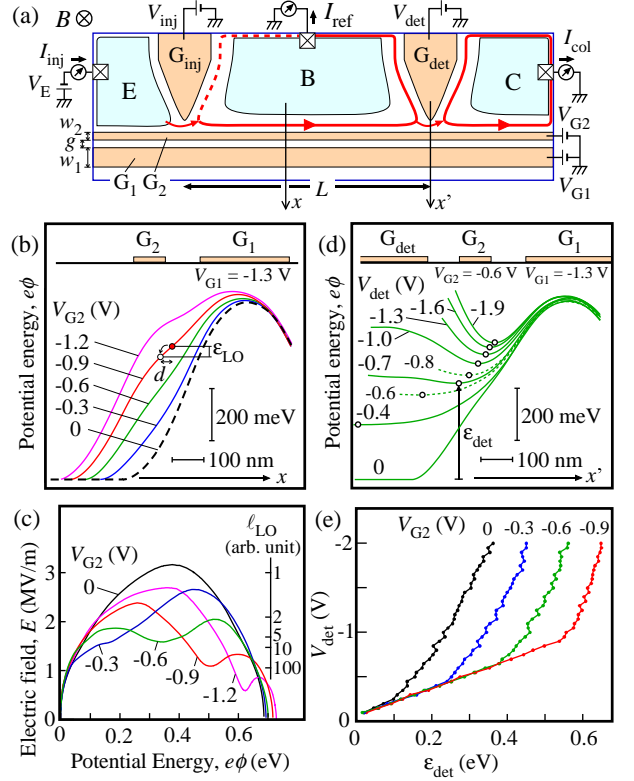


FIG. 1. (a) An experimental setup for hot-electron spectroscopy on an edge channel formed by a double gate, G_1 and G_2 . (b) Potential energy profile $e\phi(x)$ of the edge channel. The locations of G_1 and G_2 in the x axis are shown on the top. (c) The electric field $E = -d\phi/dx$ as a function of the potential energy $e\phi$. The LO-phonon scattering length ℓ_{LO} in an arbitrary unit for $B = 9$ T is shown. (d) Approximate potential energy profile $e\phi(x')$ at the detector point contact. The locations of G_1 , G_2 , and G_{det} in the x' axis are shown. (e) The detector energy ε_{det} (in the horizontal axis) as a function of V_{det} (in the vertical axis) for several V_{G2} values. Plots in (b)-(e) were obtained by numerically solving the Poisson equation with a 2D finite-element method by assuming translational invariance along the transport direction. The surface potential is fixed at $eV_g + 0.6$ eV in the gated region, but surface electron density is fixed at $6 \times 10^{11} \text{ cm}^{-2}$ in the ungated region. A uniform donor density of $9 \times 10^{11} \text{ cm}^{-2}$ is assumed. Experimental geometry with $w_1 = 280$ nm, $w_2 = 100$ nm, and $g = 100$ nm, were used in the simulation.

characteristics to confirm the double gate action.

The double gate devices with G_1 of width $w_1 = 280$ nm and G_2 of $w_2 = 100$ nm separated by gap $g = 100$ nm were fabricated by patterning a Ti layer on an Al-GaAs/GaAs heterostructure. The two-dimensional electron system located at 100 nm below the surface has an electron density of $2.7 \times 10^{11} \text{ cm}^{-2}$ and low-temperature mobility of about $10^6 \text{ cm}^2/\text{Vs}$. Under the perpendicular magnetic field of $B = 9$ T, appropriate gate voltages were applied to form injection and detection point contacts as illustrated in Fig. 1(a). While the bulk is conductive

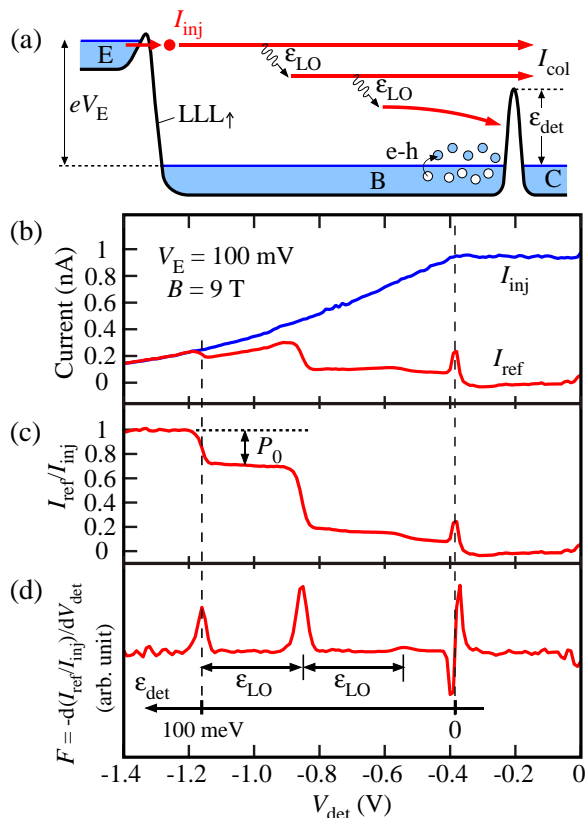


FIG. 2. (a) Schematic energy diagram of the hot-electron spectroscopy. (b) I_{ref} and I_{inj} , (c) $I_{\text{ref}}/I_{\text{inj}}$, and (d) $F = -d(I_{\text{ref}}/I_{\text{inj}})/dV_{\text{det}}$ as a function of V_{det} for $L = 2 \mu\text{m}$ device. The equispaced peaks in (d) represent the ballistic transport (the leftmost peak) and its phonon replicas. The step height P_0 in (c) measures the probability of ballistic transport.

with Landau filling factor $\nu = 1.3$, this should not influence the hot-electron transport that is well isolated from the cold electrons in the edge and the bulk [14]. We investigated two devices with the distance $L = 2$ and $4 \mu\text{m}$ between the injector and detector point contacts, and both devices show similar results. The following data was taken with the $L = 2 \mu\text{m}$ device at 1.5 K .

Figure 2(b) shows a representative data of injection current I_{inj} and reflected current I_{ref} as a function of the detector gate voltage V_{det} at $eV_{\text{E}} = 100 \text{ meV}$. We adjusted V_{inj} to provide $I_{\text{inj}} \simeq 1 \text{ nA}$ at $V_{\text{det}} = 0$, and swept V_{det} to measure the current profile. While the application of negative V_{det} slightly reduces the injection current due to the electrostatic coupling, the reflected current I_{ref} increases and eventually reaches the value identical to I_{inj} when a large barrier is formed at the detector. We confirmed that the total current is always conserved, i.e., $I_{\text{inj}} = I_{\text{col}} + I_{\text{ref}}$ (not shown). The step-like features in the normalized current $I_{\text{ref}}/I_{\text{inj}}$ in Fig. 2(c) are associated with the emission of LO phonons with $\varepsilon_{\text{LO}} = 36 \text{ meV}$. The height of the first step, P_0 , in $I_{\text{ref}}/I_{\text{inj}}$ measures the probability (fraction) that the injected electron

reaches the collector ballistically without emitting LO phonons. This is evaluated with scattering length ℓ_{LO} defined by the relation $P_0 = \exp(-L/\ell_{\text{LO}})$. The derivative $F = -d(I_{\text{ref}}/I_{\text{inj}})/dV_{\text{det}}$ in Fig. 2(d) is proportional to the energy distribution function of the edge state [14]. The three peaks at $V_{\text{det}} \simeq -1.16, -0.84, \text{ and } -0.54 \text{ V}$ are equally spaced with the separation ($\sim 0.31 \text{ V}$) corresponding to $\varepsilon_{\text{LO}} = 36 \text{ meV}$ in energy. This indicates linear $\varepsilon_{\text{det}} - V_{\text{det}}$ dependence in this energy range with a lever-arm factor $\alpha = \Delta\varepsilon_{\text{det}}/\Delta V_{\text{det}} \simeq 0.12e$. The peak in I_{ref} (the dip and peak in F) at $V_{\text{det}} \simeq -0.38 \text{ V}$ originates from electrical noise in the collector, where the noise could be rectified by the nonlinear characteristics of the point contact. Nevertheless, this marks the condition where the detector barrier is effectively zero ($\varepsilon_{\text{det}} = 0$). Considering that the peak position at $V_{\text{det}} \simeq -0.54 \text{ V}$ corresponds to the energy of $eV_{\text{E}} - 2\varepsilon_{\text{LO}} = 28 \text{ meV}$, slightly larger lever-arm factor $\alpha \simeq 0.18e$ is suggested in the low energy range of $-0.54 \text{ V} < V_{\text{det}} < -0.38 \text{ V}$. The difference in the lever-arm factor becomes larger when finite $V_{\text{G}2}$ is applied as shown below.

Figure 3 shows color plots of F as a function of V_{det} and the injection energy eV_{E} . The data taken at $V_{\text{G}2} = 0 \text{ V}$ [Fig. 3(a)] reveal several peaks, including the topmost ballistic signal and its phonon replicas. The topmost peak follows the ballistic condition ($\varepsilon_{\text{det}} = eV_{\text{E}}$), shown by the dashed line by assuming linear dependence of V_{det} on ε_{det} , for $V_{\text{E}} > 60 \text{ mV}$. The amplitude of the ballistic peak decreases with increasing eV_{E} as the LO phonon scattering rate increases with the electric field E at higher energy [14]. In contrast, the topmost peak for $V_{\text{E}} < 50 \text{ mV}$ deviates from the ballistic condition and disappears at $V_{\text{E}} = V_{\text{th}} \simeq 30 \text{ mV}$. This is associated with electron-electron scattering which becomes more significant at lower energy; indeed, the threshold energy eV_{th} is comparable to the value in our previous report [14]. In the following, we focus on the LO phonon scattering observed at $V_{\text{E}} > 60 \text{ mV}$.

The hot-electron spectrum changes dramatically when $V_{\text{G}2} = -0.3 \text{ V}$ is applied as shown in Fig. 3(b). While the ballistic peak and its phonon replicas are seen, their peak positions in V_{det} deviate significantly from those in Fig. 3(a). Clear bending is seen at $V_{\text{det}} \simeq -0.65 \text{ V}$ marked by the horizontal dashed line. This is qualitatively consistent with the electrostatic calculation of Fig. 1(e). By assuming that the topmost ballistic peak follows $\varepsilon_{\text{det}} = eV_{\text{E}}$ for $V_{\text{E}} > 60 \text{ mV}$, ε_{det} should change with V_{det} in a non-linear way as shown by the subsidiary scale in Fig. 3(b). Similar bending appears in a wide range of $V_{\text{G}2}$ as summarized in Figs. 4(a) and 4(c), where the position of the ballistic peak is plotted as a function of eV_{E} for several $V_{\text{G}2}$ values in Fig. 4(a) and for several $V_{\text{G}1}$ values in Fig. 4(c). The bending position changes with $V_{\text{G}2}$ and $V_{\text{G}1}$ in qualitative agreement with the electrostatic calculation. Note that peak positions of the phonon-replicas also show bending (not shown) at the same position in V_{det} as the ballistic peak position, indicating that the bending originates in the detector. This ensures that the

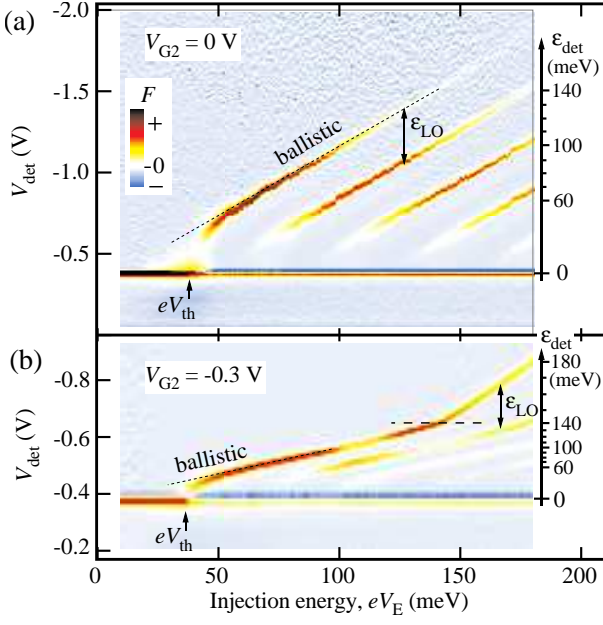


FIG. 3. Representative hot-electron spectrum F as a function of V_{det} for various eV_E taken at $V_{G2} = 0$ V in (a) and $V_{G2} = -0.3$ V in (b). The data was taken at $B = 9$ T (the bulk filling factor $\nu = 1.3$) and $V_{G1} = -1.3$ V. The subsidiary scale of ε_{det} is determined from the ballistic peak position for $eV_E > 60$ meV.

edge potential is modulated with V_{G2} .

The peak height (color) of the ballistic signal plotted in Fig. 3(b) shows a complicated dependence on V_E , with two maxima at $V_E \simeq 70$ and 130 mV. While the first maximum at $V_E \simeq 70$ mV should be explained with the electron-electron scattering as in Fig. 3(a), the second maximum at $V_E \simeq 130$ mV close to the bending position indicates the reduction of LO phonon scattering rate. The step height P_0 in $I_{\text{ref}}/I_{\text{inj}}$ of Fig. 2(c), which measures the probability of the ballistic transport over the channel length L , is plotted as a function of the injection energy eV_E (> 60 meV) for several V_{G2} values in Fig. 4(b) and for several V_{G1} values in Fig. 4(d). Corresponding scattering length ℓ_{LO} is shown on the right scale. While P_0 and thus ℓ_{LO} monotonically decrease with eV_E at $V_{G2} = 0$ in Fig. 4(b), non-monotonic dependence of P_0 with a broad peak, marked by triangles, is seen at negative V_{G2} . The peak position moves to the high energy side by making V_{G2} more negative. This behavior is qualitatively consistent with that of the dip position in E [Fig. 1(c)]. Similarly, the peak position moves to the high energy side by making V_{G1} more negative in Fig. 4(b), which is also consistent with the simulation (not shown). In this way, we have successfully modified the edge potential and the LO phonon scattering length with the double gate geometry.

The modulation of the edge potential may also influence the electron-electron scattering in the low energy region ($eV_E < 60$ meV). Several competing effects are ex-

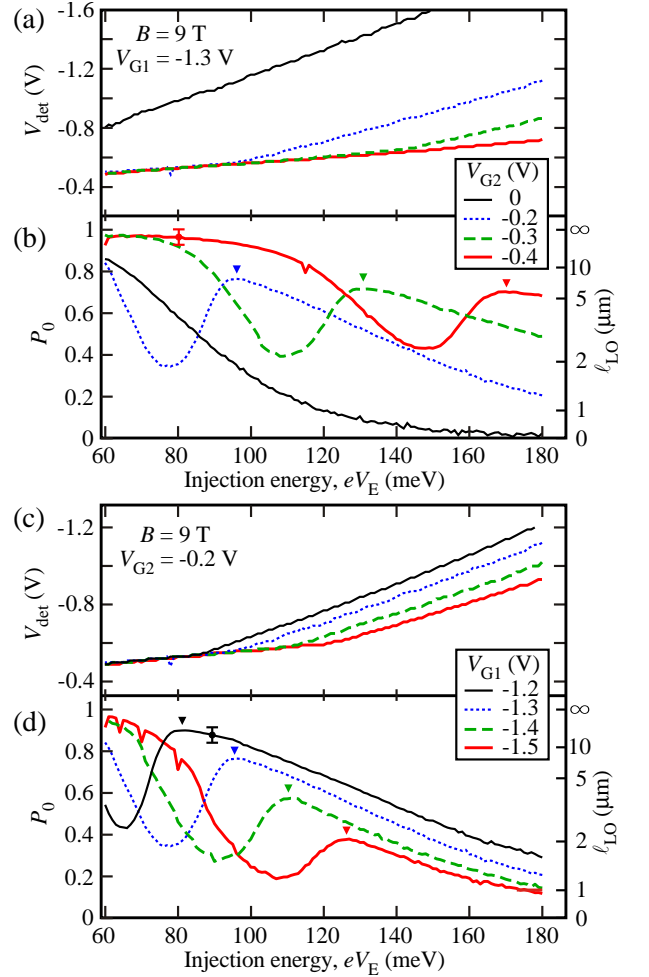


FIG. 4. Injection energy (eV_E) dependence of the ballistic peak position in V_{det} in (a) and (c) and the ballistic transport probability P_0 in (b) and (d) for several V_{G2} values at $V_{G1} = -1.3$ V in (a) and (b) and for several V_{G1} values at $V_{G2} = -0.2$ V in (c) and (d). The corresponding scattering length ℓ_{LO} is shown in the right scale of (b) and (d). The triangles mark the enhancement of P_0 (and thus ℓ_{LO}) with the gentle edge potential. A representative error bar is shown in (b) and (d).

pected [14]. When the potential slope is made less steep, the hot electron velocity decreases toward the single-particle velocity at the Fermi energy, which would contribute to increase the electron-electron scattering rate as the energy and momentum conservation is met at equal velocities. On the other hand, the hot electrons become spatially more separated from the Fermi sea, which would work to decrease the scattering rate. While these two effects cancel each other for a simplified potential profile $\phi \propto x^\xi$ with an exponent ξ and the unscreened Coulomb potential, the scattering rate for the potential modified by V_{G2} in our device may change. In addition, screening by the gate metal can suppress the electron-electron scattering. Experimentally we did not see clear V_{G2} dependence in the electron-electron scattering and the thresh-

old energy eV_{th} at which the hot electron peak starts to appear in Fig. 3. Further studies are encouraged on this effect.

In summary, we have demonstrated that the edge potential can be modulated with a double gate geometry by measuring the LO phonon scattering length. This scheme may be useful in extending the ballistic length and tuning the charge velocity, and can be extended for

fully depleted regions with more than two gates. This is attractive for studying electronic analog of quantum optics with hot electrons.

We thank Tomoaki Ota, Masayuki Hashisaka and Tokuro Hata for fruitful discussions and supports. This work was supported by JSPS KAKENHI (JP26247051, JP15H05854, JP17K18751, JP19H05603), and Nanotechnology Platform Program of MEXT.

-
- [1] Yu. V. Nazarov and Y. M. Blantar, *Quantum Transport: Introduction to Nanoscience*, Cambridge Univ. Press (2009).
- [2] C. W. J. Beenakker and H. van Houten, *Quantum Transport in Semiconductor Nanostructures*, *Solid State Physics*, **44**, 1 (1991).
- [3] Y. Hirayama, T. Saku, S. Tarucha, and Y. Horikoshi, Ballistic electron transport in macroscopic four-terminal square structures with high mobility, *Appl Phys. Lett.* **58**, 2672 (1991).
- [4] B. I. Halperin, Quantized Hall conductance, current-carrying edge states, and the existence of extended states in a two-dimensional disordered potential, *Phys. Rev. B* **25**, 2185 (1982).
- [5] Z. F. Ezawa, *Quantum Hall Effects: Field Theoretical Approach and Related Topics*, World Scientific (2008).
- [6] Y. Ji, Y. Chung, D. Sprinzak, M. Heiblum, and D. Mahalu, An electronic Mach Zehnder interferometer, *Nature* **422**, 415 (2003).
- [7] V. Freulon, A. Marguerite, A. Cavanna, Y. Jin, and G. Fève, Hong-Ou-Mandel experiment for temporal investigation of single-electron fractionalization, *Nature Commun.* **6**, 6854 (2015).
- [8] R. Bisognin, A. Marguerite, B. Roussel, M. Kumar, C. Cabart, C. Chapdelaine, A. Mohammad-Djafari, J.-M. Berroir, E. Bocquillon, B. Plaçais, A. Cavanna, U. Gennser, Y. Jin, P. Degiovanni and G. Fève, Quantum tomography of electrical currents, *Nature Commun.* **10**, 3379 (2019).
- [9] D. Taubert, C. Tomaras, G. J. Schinner, H. P. Tranitz, W. Wegscheider, S. Kehrein, and S. Ludwig, Relaxation of hot electrons in a degenerate two-dimensional electron system: Transition to one-dimensional scattering, *Phys. Rev. B* **83**, 235404 (2011).
- [10] K. Itoh, R. Nakazawa, T. Ota, M. Hashisaka, K. Muraki, and T. Fujisawa, Signatures of a nonthermal metastable state in copropagating quantum Hall edge channels, *Phys. Rev. Lett.* **120**, 197701 (2018).
- [11] T. Krähenmann, S. G. Fischer, M. Rösli, T. Ihn, C. Reichl, W. Wegscheider, K. Ensslin, Y. Gefen, and Y. Meir, Auger-spectroscopy in quantum Hall edge channels and the missing energy problem, *Nature Commun.* **10**, 3915 (2019).
- [12] R. H. Rodriguez, F.D. Parmentier, P. Roulleau, U. Gennser, A. Cavanna, F. Portier, D. Mailly, P. Roche, Strong energy relaxation of propagating quasiparticles in the quantum Hall regime, arXiv:1903.05919
- [13] H. Duprez, E. Sivre, A. Anthore, A. Aassime, A. Cavanna, A. Ouerghi, U. Gennser, and F. Pierre, Macroscopic Electron Quantum Coherence in a Solid-State Circuit, *Physical Review X* **9**, 021030 (2019).
- [14] T. Ota, S. Akiyama, M. Hashisaka, K. Muraki, and T. Fujisawa, Spectroscopic study on hot-electron transport in a quantum Hall edge channel, *Phys. Rev. B* **99**, 085310 (2019).
- [15] N. Johnson, C. Emary, S. Ryu, H.-S. Sim, P. See, J. D. Fletcher, J. P. Griffiths, G. A. C. Jones, I. Farrer, D. A. Ritchie, M. Pepper, T. J. B. M. Janssen, and M. Kataoka, LO-phonon emission rate of hot electrons from an on demand single-electron source in a GaAs/AlGaAs heterostructure, *Phys. Rev. Lett.* **121**, 137703 (2018).
- [16] C. Bäuerle, D. C. Glatli, T. Meunier, F. Portier, P. Roche, P. Roulleau, S. Takada and X. Waintal, Coherent control of single electrons: a review of current progress, *Rep. Prog. Phys.* **81**, 056503 (2018).
- [17] J. D. Fletcher, P. See, H. Howe, M. Pepper, S. P. Giblin, J. P. Griffiths, G. A. C. Jones, I. Farrer, D. A. Ritchie, T. J. B. M. Janssen, and M. Kataoka, Clock-controlled emission of single-electron wave packets in a solid-state circuit, *Phys. Rev. Lett.* **111**, 216807 (2013).
- [18] M. Kataoka, N. Johnson, C. Emary, P. See, J. P. Griffiths, G. A. C. Jones, I. Farrer, D. A. Ritchie, M. Pepper, and T. J. B. M. Janssen, Time-of-flight measurements of single-electron wave packets in quantum Hall edge states, *Phys. Rev. Lett.* **116**, 126803 (2016).
- [19] J. D. Fletcher, N. Johnson, E. Locane, P. See, J. P. Griffiths, I. Farrer, D. A. Ritchie, P. W. Brouwer, V. Kashcheyevs, and M. Kataoka, Quantum tomography of solitary electrons (2019), arXiv:1901.10985.
- [20] L. Freise, T. Gerster, D. Reifert, T. Weimann, K. Pierz, F. Hohls, and N. Ubbelohde, Full counting statistics of trapped ballistic electrons (2019), arXiv:1902.11253.
- [21] N. Ubbelohde, F. Hohls, V. Kashcheyevs, T. Wagner, L. Fricke, B. Kaestner, K. Pierz, H. W. Schumacher, and R. Haug, Partitioning of on-demand electron pairs, *Nature Nanotech.* **10**, 46 (2014).
- [22] C. Emary, L. A. Clark, M. Kataoka, and N. Johnson, Energy relaxation in hot electron quantum optics via acoustic and optical phonon emission, *Phys. Rev. B* **99**, 045306 (2019).
- [23] H. Kamata, N. Kumada, M. Hashisaka, K. Muraki, and T. Fujisawa, Fractionalized wave packets from an artificial Tomonaga-Luttinger liquid, *Nature Nanotech.* **9**, 177 (2014).
- [24] M. Hashisaka, N. Hiyama, T. Akiho, K. Muraki and T. Fujisawa, Waveform measurement of charge- and spin-density wavepackets in a chiral Tomonaga-Luttinger liquid, *Nature Phys.* **13**, 559 (2017).
- [25] J. H. Davies and I. A. Larkin, Theory of potential modulation in lateral surface superlattices, *Phys. Rev. B* **49**, 4800 (1994).
- [26] S. Komiyama, H. Hirai, M. Ohsawa, Y. Matsuda, S. Sasa,

and T. Fujii, Inter-edge-state scattering and nonlinear

effects in a two-dimensional electron gas at high magnetic Fields, Phys. Rev. B **45**, 11085 (1992).